The Astrophysical Journal Letters, 811:L23 (5pp), 2015 October 1 doi:10.1088/2041-8205/811/2/L23

A NEW CONSTRAINT ON THE MOLECULAR OXYGEN ABUNDANCE AT $z \sim 0.886$

Nissim Kanekar[1,3] and David S. Meier[2]
[1] National Centre for Radio Astrophysics, Tata Institute of Fundamental Research, Ganeshkhind, Pune-411007, India; nkanekar@ncra.tifr.res.in
[2] Department of Physics, New Mexico Institute of Mining and Technology, 801 Leroy Place, Socorro, NM 87801, USA
Received 2015 August 4; accepted 2015 August 28; published 2015 September 24

ABSTRACT

We report Karl G. Jansky Very Large Array (VLA) and Atacama Large Millimeter/submillimeter Array (ALMA) spectroscopy in the redshifted molecular oxygen (O_2) 56.265 and 424.763 GHz transitions from the $z = 0.88582$ gravitational lens toward PKS 1830−21. The ALMA non-detection of O_2 424.763 GHz absorption yields the 3σ upper limit $N(O_2) \leqslant 5.8 \times 10^{17}$ cm^{-2} on the O_2 column density, assuming that the O_2 level populations are thermalized at the gas kinetic temperature of 80 K. The VLA spectrum shows absorption by the CH_3CHO 56.185 and 56.265 GHz lines, with the latter strongly blended with the O_2 56.265 GHz line. Since the two CH_3CHO lines have the same equilibrium strength, we used the known CH_3CHO 56.185 GHz line profile to subtract out the CH_3CHO 56.265 GHz feature from the VLA spectrum, and then carried out a search for O_2 56.265 GHz absorption in the residual spectrum. The non-detection of redshifted O_2 56.265 GHz absorption in the CH_3CHO-subtracted VLA spectrum yields $N(O_2) \leqslant 2.3 \times 10^{17}$ cm^{-2}. Our 3σ limits on the O_2 abundance relative to H_2 are then $X(O_2) \leqslant 9.1 \times 10^{-6}$ (VLA) and $X(O_2) \leqslant 2.3 \times 10^{-5}$ (ALMA). These are 5–15 times lower than the best previous constraint on the O_2 abundance in an external galaxy. The low O_2 abundance in the $z = 0.88582$ absorber may arise due to its high neutral carbon abundance and the fact that its molecular clouds appear to be diffuse or translucent clouds with low number density and high kinetic temperature.

Key words: galaxies: individual (PKS 1830–21) – ISM: abundances – quasars: absorption lines

1. INTRODUCTION

Molecular oxygen (O_2) has long been identified as a critical species for the understanding of cooling and energy balance in molecular clouds, and of interstellar chemistry (e.g., Goldsmith & Langer 1978; Goldsmith et al. 2011). In standard models of chemistry, the O_2 abundance relative to that of molecular hydrogen H_2 is expected to rise to $X(O_2) \equiv N(O_2)/N(H_2) \sim 10^{-5}$, comparable to the carbon monoxide abundance, at times beyond $\sim 3 \times 10^5$ years (e.g., Herbst & Klemperer 1973; Marechal et al. 1997). Remarkably, despite numerous searches with the *Submillimeter Wave Astronomy Satellite*, and the *Odin* and *Herschel* satellites, O_2 has been detected in only two directions in the Galaxy, toward ρOph A (Larsson et al. 2007; Liseau et al. 2012) and Orion H_2 Peak 1 (Goldsmith et al. 2011; Chen et al. 2014), with abundances $X(O_2) \approx 5 \times 10^{-8}$ (ρOph A; Larsson et al. 2007; Liseau et al. 2012) and $\approx 10^{-6}$ (Orion H_2 Peak 1, whose relatively high abundance has been explained as arising due to a low-velocity C-type shock, with a modest far-ultraviolet radiation field Goldsmith et al. 2011; Chen et al. 2014; Melnick & Kaufman 2015). The majority of searches have yielded low O_2 abundances in both diffuse and dark clouds, $X(O_2) < 10^{-7}$ (e.g., Pagani et al. 2003; Yıldız et al. 2013), two orders of magnitude lower than expected. Although many attempts have been made to explain the paucity of O_2 (e.g., Bergin et al. 2000; Charnley et al. 2001; Quan et al. 2008; Hollenbach et al. 2009; Whittet 2010), the low O_2 abundances in molecular clouds remain a serious problem for models of chemistry.

For cosmologically distant galaxies, the O_2 lines are redshifted outside the telluric bands and can be observed with ground-based telescopes. Unlike satellite-based O_2 *emission* searches, where the large telescope beam means that the derived $X(O_2)$ is an average over multiple molecular clouds, searches for O_2 in *absorption* toward compact radio sources provide estimates of $X(O_2)$ in individual clouds along the sightline. Such observations are especially interesting for high-z systems as they allow studies of interstellar chemistry in much younger galaxies.

The two best targets for a search for redshifted O_2 in absorption are the spiral gravitational lenses at $z \sim 0.685$ and $z \sim 0.886$ toward B0218+357 and PKS 1830–21, respectively, which show absorption in a variety of molecular species (e.g., Wiklind & Combes 1995, 1996, 1998; Combes & Wiklind 1997; Chengalur et al. 1999; Kanekar et al. 2003; Henkel et al. 2005; Muller et al. 2014). Molecular absorption studies of these galaxies have been used to determine physical conditions in the absorbing clouds (e.g., Henkel et al. 2008; Menten et al. 2008), to estimate the temperature of the microwave background (e.g., Muller et al. 2013), and even to constrain changes in the fundamental constants of physics (e.g., Kanekar 2011; Bagdonaite et al. 2013; Kanekar et al. 2015).

Searches for O_2 absorption have been carried out at $z = 0.685$ toward B0218+357 in the O_2 368 and 424 GHz transitions (Combes & Wiklind 1995) and the O_2 56 and 119 GHz transitions (Combes et al. 1997). These yielded the upper limit $N(O_2) < 2.9 \times 10^{18}$ cm^{-2} on the O_2 column density, where we have updated the results of Combes et al. (1997) for an O_2 excitation temperature equal to the inferred gas kinetic temperature (55 K; Henkel et al. 2005). The H_2 column density of the $z \sim 0.685$ absorber is $\approx 2 \times 10^{22}$ cm^{-2} (Gerin et al. 1997; Kanekar & Chengalur 2002); this yields $X(O_2) \leqslant 1.5 \times 10^{-4}$, three orders of magnitude poorer than the limits from Galactic studies (e.g., Pagani et al. 2003).

We have used the Karl G. Jansky Very Large Array (VLA) and the Atacama Large Millimeter/submillimeter Array (ALMA) to search for redshifted O_2 absorption in the $z = 0.886$ spiral lens toward PKS 1830−21. In this Letter,

[3] Swarnajayanti Fellow.

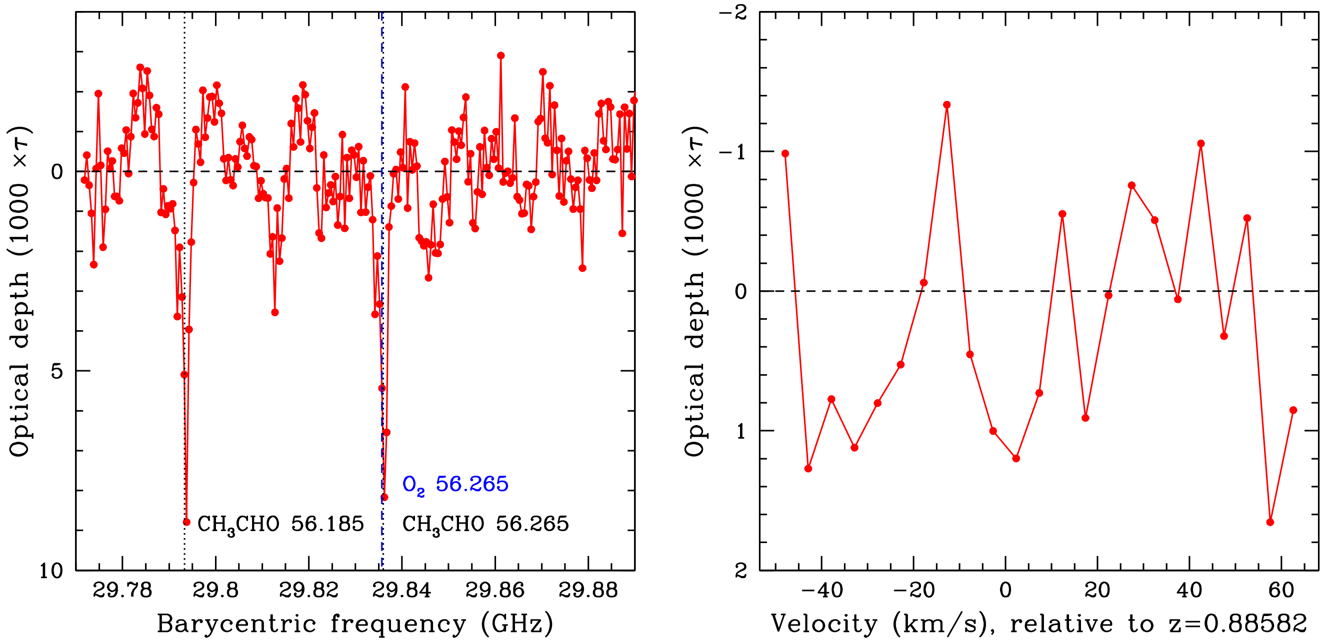

Figure 1. Left panel: the final VLA spectrum toward PKS 1830−21, with optical depth against the S–W component (in units of $1000 \times \tau$) plotted against barycentric frequency, in GHz. The dashed vertical line indicates the redshifted O_2 56 GHz line frequency, while the dotted vertical lines indicate the redshifted frequencies of the two CH_3CHO lines (one of which is in excellent agreement with the O_2 frequency). Right panel: the residual VLA spectrum, with optical depth plotted vs. velocity (in km s^{-1}, relative to $z = 0.88582$), covering the velocities around the redshifted O_2 56 GHz line frequency after subtracting out the CH_3CHO 56.185 GHz line profile from the spectrum.

we report results from our observations, which yield stringent constraints on the O_2 abundance in this galaxy.

2. OBSERVATIONS, DATA ANALYSIS, AND RESULTS

2.1. VLA Observations

The Ka-band receivers of the VLA were used in 2010 July to carry out a search for $O_2\, 1_2 \rightarrow 1_1$ 56.2648 GHz absorption at $z = 0.88582$ toward PKS 1830−21 (proposal 10A-110). The observations used the WIDAR correlator as the backend, with a single 128 MHz band, sub-divided into 256 channels, centered at the redshifted O_2 line frequency of 29.835 GHz, and two circular polarizations. Observations of 3C286 and the bright sources 3C273 and J2253+1608 were used to calibrate the flux density scale and the system bandpass, respectively. The total on-source time was 2 hr, with 19 working antennas in the VLA C-configuration.

The VLA data were analyzed in "classic" AIPS using standard procedures. Note that PKS 1830−21 is unresolved by our 19-antenna VLA C-array at Ka-band. After initial calibration, the tasks UVSUB and UVLIN were used to subtract the image of PKS 1830−21 from the calibrated visibilities, and then to subtract out any residual continuum by fitting a linear baseline to line-free channels. The residual visibilities were then imaged and the final spectrum covering the redshifted O_2 56.265 GHz transition obtained by taking a cut through the spectral cube at the location of PKS 1830−21.

The final VLA spectrum is shown in the left panel of Figure 1, with optical depth against the S–W image component of PKS 1830−21 plotted versus heliocentric frequency, in GHz. The root mean square (rms) noise on the spectrum is $\approx 1.1 \times 10^{-3}$ per 5 km s^{-1} channel, in optical depth units (assuming that the S–W component contains ≈ 38% of the total flux density of PKS 1830−21 at these frequencies; e.g., Muller et al. 2011). A strong absorption feature, with an integrated optical depth of $\approx(0.146 \pm 0.014)$ km s^{-1}, is clearly visible at the expected frequency of the redshifted O_2 56.265 GHz line (indicated by the dashed vertical line). However, it was realized that there is a CH_3CHO transition ($3_{-1,3} \rightarrow 2_{-1,2}$ E) at a rest frequency of 56.2652 GHz that would be strongly blended with the O_2 56.265 GHz line, and that might cause the observed absorption. Further, a second absorption feature is visible at ≈29.793 GHz, which could be redshifted CH_3CHO absorption, in the $3_{1,3} \rightarrow 2_{1,2}$ A++ transition. If the two features indeed arise from CH_3CHO, it would be difficult to draw conclusions about the O_2 abundance (although see below). We hence carried out an ALMA search for redshifted O_2 424 GHz absorption, to test whether the VLA absorption feature indeed arises from the O_2 56.265 GHz line.

2.2. ALMA Observations

The Band-6 receivers of ALMA were used in 2014 March to search for redshifted $O_2\, 1_2 \rightarrow 3_2$ 424.7631 GHz absorption at $z = 0.88582$ toward PKS 1830−21. The observations used four 1.875 GHz intermediate frequency (IF) bands, each sub-divided into 3840 channels, and with two polarizations. The four IF bands were centered at 225.780 GHz (covering the redshifted O_2 424 GHz line frequency), 228.530, 241.033 and 243.733 GHz. Observations of Titan, J1733−1304, J1923−2104, and a few calibrators were used to calibrate the flux density scale and the system bandpass and gain. The total on-source time was ≈ 2 hr, with 25 ALMA antennas.

The ALMA data were analyzed in two stages, first using the CASA pipeline to carry out the initial calibration procedure, and then self-calibrating the data of PKS 1830−21 in AIPS. The flux density scale was calibrated using the short-baseline data on Titan, and this was then extended to longer baselines by bootstrapping the data of J1923−2104.

The data of J1733−1304 and J1923−2104 were, respectively, used to calibrate the system bandpass and initial gain. After applying the initial calibration in CASA, a standard self-calibration procedure was used in AIPS, with a few rounds of phase-only self-calibration followed by a single round of amplitude-and-phase self-calibration. The final image has a synthesized beam of ≈1.″0 × 0.″8 (with the two strong image components of PKS 1830−21 marginally resolved), and an rms noise of ≈ 0.14 mJy Beam^{-1}. The task JMFIT was used to measure the flux densities of the N–E and S–W image components, via a 2-Gaussian fit to the final image; this yielded flux densities of 549.98 ± 0.43 mJy (N–E) and 342.63 ± 0.43 mJy (S–W). The continuum image of PKS 1830−21 was then subtracted from the calibrated visibilities of each IF band using the task UVSUB, and the residual visibilities of each band were then imaged to produce a spectral cube, after shifting the data to the heliocentric frame. The spectrum for each IF band was then produced via a cut through the cube at the location of the S–W image component. The final spectra have an rms noise of ≈ 1.0–1.3 mJy at the re-sampled velocity resolution of ≈ 1.3 km s^{-1}.

The final Hanning-smoothed and re-sampled spectra from the four ALMA IF bands (after subtracting a second-order baseline) against the S–W component are shown in the four panels of Figure 2, with optical depth plotted versus heliocentric frequency, in GHz. All spectra are shown after smoothing to, and re-sampling at, a velocity resolution of ≈6.5 km s^{-1} the resolution at which the search for redshifted O_2 424 GHz absorption was carried out. No evidence for O_2 424 GHz absorption can be discerned in the spectrum in the top left panel of Figure 2. The final rms noise on the spectrum is ≈1.8×10^{-3} per 6.5 km s^{-1} channel, in optical depth units.

In passing, we note that four absorption features were clearly detected in the ALMA spectra; three of these correspond to the CO (4–3) and two CN (4–3) transitions (see Figure 2). However, we have been unable to identify the fourth transition, at ≈ 226.033 GHz, i.e., at rest-frame frequencies of 426.257 GHz (at $z = 0.88582$, the absorber being studied here), 792.698 GHz (at $z = 2.507$, the redshift of PKS 1830−21; Lidman et al. 1999) or 269.567 GHz (at $z = 0.1926$, the redshift of another known absorber toward PKS 1830−21; Lovell et al. 1996). The line width is ≈ 5 km s^{-1}, similar to that of other high-frequency transitions from the $z = 0.88582$ absorber. It appears that this is not a known low-energy transition of a species expected to be abundant in the ISM.

3. DISCUSSION

The first question is whether the absorption feature seen at ≈29.836 GHz in the VLA spectrum of PKS 1830−21 arises from O_2 or from CH_3CHO (or, indeed, some other transition). The lower energy level of the O_2 56 GHz and O_2 424 GHz transitions is the same (the 1_2 state; see Figure 3), permitting a direct comparison between the expected optical depths in the two lines. Of course, the ratio of the line strengths depends on the respective excitation temperatures. In the case of the $z = 0.88582$ absorber, the number density n_{H_2} and kinetic temperature T_k of the molecular gas have been estimated to be $n_{H_2} \sim 1700$–2600 cm^{-3} and $T_k \approx 80$ K (Henkel et al. 2008, 2009). For number densities $\gtrsim 10^3$ cm^{-3} and $T_k \geqslant 30$ K, the O_2 line populations are expected to be thermalized (e.g., Goldsmith et al. 2000), i.e., $T_x \approx T_k$. For $T_x \approx 80$ K, the 424 GHz line is expected to be slightly stronger than the 56 GHz line, $\tau_{424} \approx 1.1 \times \tau_{56}$. Our ALMA 3$\sigma$ limit on the integrated O_2 424 GHz optical depth is ≈ 0.037 km s^{-1}, a factor of 5 lower than the integrated optical depth (≈ 0.146 ±0.014 km s^{-1}) of the 29.836 GHz absorption feature in the VLA spectrum. We can thus conclusively rule out the possibility that the VLA absorption feature arises from the O_2 56 GHz transition. The feature is most likely to arise from the CH_3CHO $3_{-1,3} \rightarrow 2_{-1,2}$ E transition.

The ALMA upper limit to the O_2 424 GHz optical depth can be used to place a limit on the total O_2 column density. For $T_x = 80$ K, this gives $N(O_2) \leqslant 5.8 \times 10^{17}$ cm^{-2}, at 3σ significance.

Interestingly, the two CH_3CHO transitions ($3_{-1,3} \rightarrow 2_{-1,2}$ E and $3_{1,3} \rightarrow 2_{1,2}$ A++) seen in the VLA spectrum at, respectively, 29.836 GHz and 29.793 GHz, have the same line strengths. One can hence subtract one from the other to search for any additional absorption arising from the O_2 56 GHz line. This was done by using two-point interpolation to resample the CH_3CHO $3_{1,3} \rightarrow 2_{1,2}$ A++ line profile at the measured velocities of the CH_3CHO $3_{-1,3} \rightarrow 2_{-1,2}$ E line, and then subtracting out the resampled line profile from the latter spectrum. This procedure is unlikely to yield any systematic effects, as both CH_3CHO line profiles are well-sampled, with at least 3 independent spectral points detected at $>5\sigma$ significance. No absorption is detected in the residual VLA spectrum, yielding an integrated O_2 56 GHz optical depth of <0.0131 km s^{-1}, again at 3σ significance, against the S–W component of PKS 1830−21. Again using $T_x = 80$ K, this yields $N(O_2) \leqslant 2.3 \times 10^{17}$ cm^{-2}, a factor of ≈ 2.5 more stringent than the ALMA upper limit.

The H_2 column density of the $z \sim 0.886$ lens has been estimated to be ≈2.5×10^{22} cm^{-2} (Gerin et al. 1997; Wiklind & Combes 1998). These are broadly consistent with estimates of the total hydrogen column density toward both lensed images from *Chandra* and *ROSAT* X-ray spectroscopy, N(H) = (1.8–3.5)×10^{22} cm^{-2} (Mathur & Nair 1997; Dai et al. 2006). Note that, while Muller & Guélin (2008) argue that the H_2 column density may be an order of magnitude larger than the above values to account for the detection of species such as $HC^{17}O^+$ and $HC^{15}N$ in absorption, such a high value of $N(H_2)$ appears to be ruled out by the X-ray data. Using a value of $N(H_2) = 2.5 \times 10^{22}$ cm^{-2} yields O_2 abundances of $X(O_2) \leqslant 9.1 \times 10^{-6}$ and $X(O_2) \leqslant 2.3 \times 10^{-5}$ from the VLA (CH_3CHO-subtracted) O_2 56 GHz and the ALMA O_2 424 GHz non-detections, respectively. Of course, if the higher H_2 column density estimate of Muller & Guélin (2008) is correct, then our constraints on the O_2 abundance would be more stringent by an order of magnitude, i.e., $X(O_2) \leqslant 9.1 \times 10^{-7}$.

Prior to this work, the strongest constraint on the O_2 abundance outside the Milky Way was $X(O_2) \leqslant 1.5 \times 10^{-4}$ in the $z = 0.685$ absorber toward B0218+357 (see Section 1; Combes et al. 1997). Our VLA upper limit on the O_2 abundance in the $z = 0.886$ absorber toward PKS 1830−21 is a factor of ≈15 lower than this, and comparable to the measured O_2 abundance toward the Orion H_2 Peak 1 (Goldsmith et al. 2011). However, our limit is nearly two orders of magnitude weaker than the constraints on, or measurements of, O_2 abundances in the Milky Way (e.g., Pagani et al. 2003; Larsson et al. 2007; Liseau et al. 2012). Unfortunately, the high gas kinetic temperatures in the two

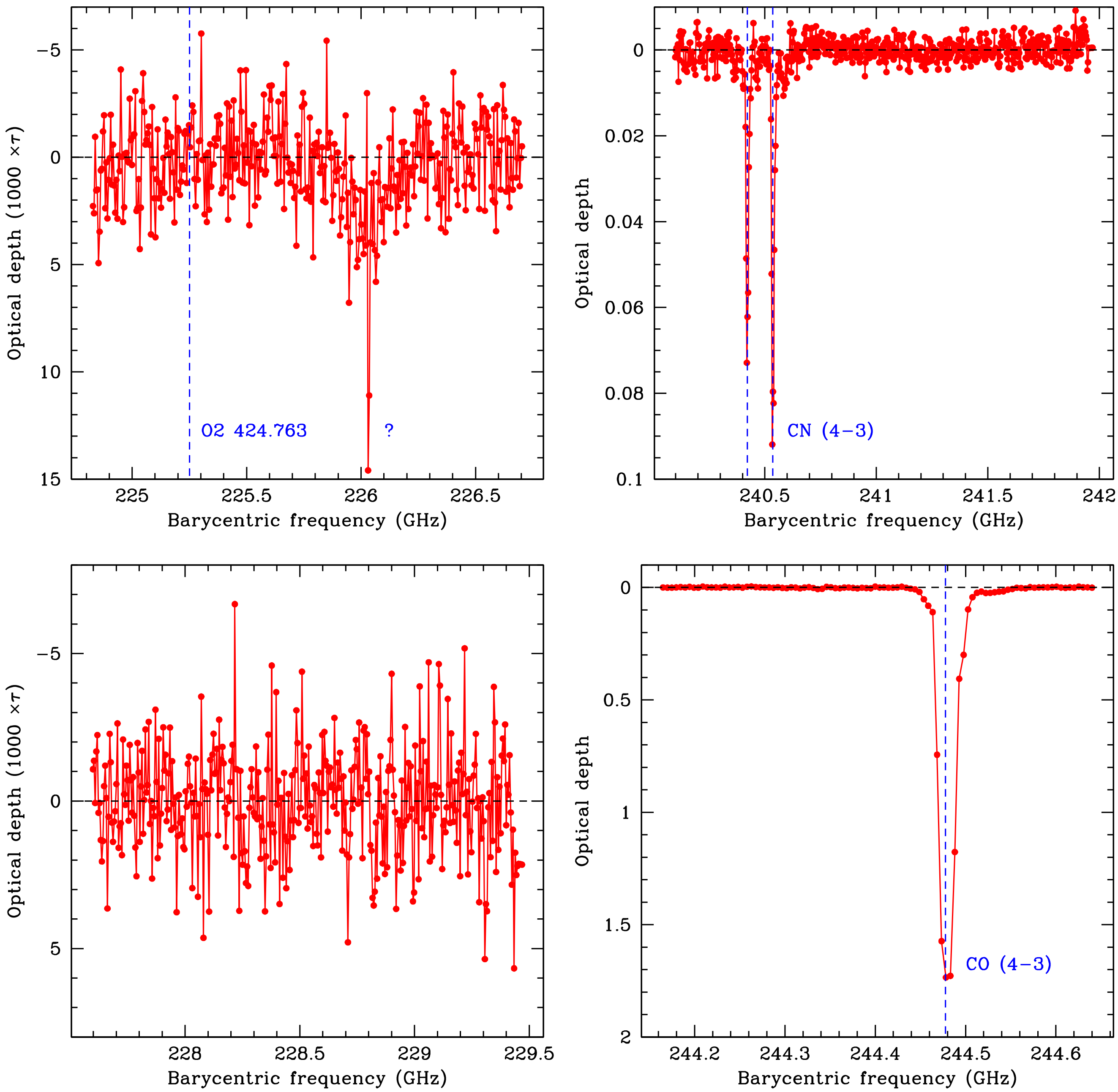

Figure 2. Spectra toward PKS 1830−21 from the four ALMA IF bands, at a velocity resolution of ≈ 6.5 km s^{-1}. The dashed vertical line in the top left panel indicates the redshifted O_2 424 GHz line frequency; no absorption is detected here. The two absorption features in the top right panel are from the CN (4–3) 453.392 and 453.607 GHz transitions, while the strong feature in the bottom right panel is the CO (4–3) transition. The transition giving rise to the absorption feature at ≈ 226.033 GHz (indicated by a question mark) in the top left panel remains unidentified.

gravitational lenses, ≈55 K in the $z = 0.685$ absorber and ≈ 80 K in the $z = 0.886$ absorber, imply that it will not be easy to improve upon our present constraint and achieve an O_2 abundance sensitivity comparable to those in the Milky Way.

While our O_2 abundance constraints for the $z = 0.88582$ absorber are less stringent than those in the Galaxy, these are by far the most sensitive constraints in an external galaxy. Further, the Galactic estimates stem from emission studies with differing angular resolution in the O_2 and CO lines. The derived abundances are hence an average over multiple molecular clouds with different excitation conditions; this can imply large uncertainties in $X(O_2)$, of upto two orders of magnitude (e.g., Liseau et al. 2010). The resolution of the present interferometric absorption study is determined by the size of the background radio continuum at the observing frequency. For PKS 1830−21, the emission from the S–W image at high frequencies (14.5–43 GHz) arises in a compact source of size <0.5 mas (Jin et al. 2003; Sato et al. 2013), i.e., transverse size <4 pc at $z = 0.88582$. The O_2 abundance estimates are hence likely to be reliable here, as both the O_2 and the H_2 column densities are inferred from absorption studies probing the same pencil beam toward the S–W image.

Finally, it is clear that we rule out O_2 abundances of $\approx 10^{-5}$ at 3σ significance in the $z = 0.886$ lens toward PKS 1830−21. As noted earlier, the O_2 abundance is expected to reach about this level, comparable to the CO abundance, in standard models

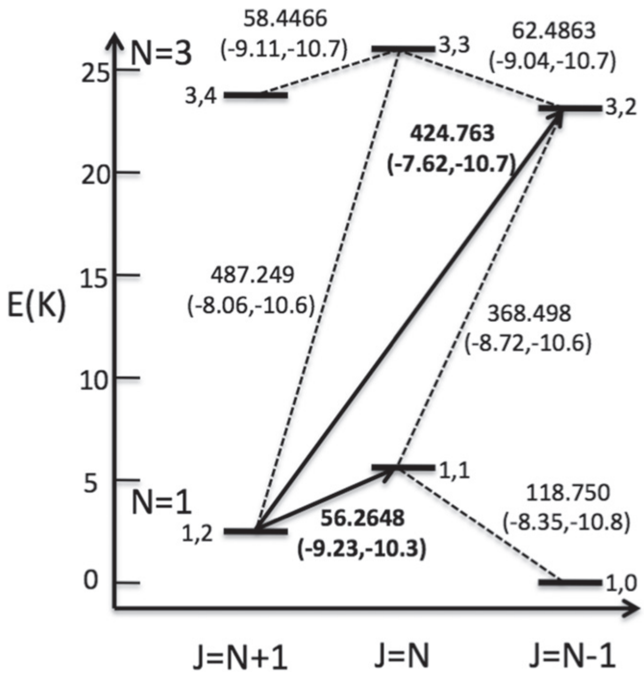

Figure 3. Low energy level diagram for O_2, adapted from Marechal et al. (1997), with levels labeled by their (N, J) quantum numbers. The observed transitions and transitions of comparable energy are displayed with solid and dashed arrows, respectively. Transition are labeled by their rest frequency (in GHz, from Splatalogue; e.g., Pickett et al. 1998; Remijan & Markwick-Kemper 2007; Drouin et al. 2010) and radiative/collisional rate coefficients (as ($\log[A_{ul}]$, $\log[C_{ul}]$), with values for C_{ul} from the RADEX database; Schöier et al. 2005; Lique 2010).

of molecular chemistry within $\approx 3 \times 10^5$ years (e.g., Herbst & Klemperer 1973; Marechal et al. 1997). The low O_2 abundance thus appears a conundrum, even for the $z = 0.886$ absorber. A possible explanation lies in the high derived abundance of neutral carbon in this system by Bottinelli et al. (2009), who obtain $N(\mathrm{C})/N(\mathrm{H_2}) \approx 10^{-4}$, somewhat larger than the CO abundance. In typical molecular clouds, O_2 is destroyed by the reactions $\mathrm{C} + \mathrm{O_2} \rightarrow \mathrm{CO} + \mathrm{O}$, $\mathrm{C^+} + \mathrm{O_2} \rightarrow \mathrm{CO} + \mathrm{O^+}$, and $\mathrm{C^+} + \mathrm{O_2} \rightarrow \mathrm{CO^+} + \mathrm{O}$. The high carbon abundance in the $z = 0.886$ absorber is thus unfavorable for the survival of O_2, and can account for its low abundance. Bottinelli et al. (2009) also note that the high carbon abundance relative to CO suggests that the absorbing gas arises in translucent clouds, or clouds in an early phase of the transition from diffuse to dense gas, with low densities and mild-UV fields. This is consistent with the high gas kinetic temperature, ($\approx$80 K), and relatively low densities ($\approx$1700–2600 $\mathrm{cm^{-3}}$) obtained by Henkel et al. (2009), implying that the absorber at $z = 0.88582$ does not arise in a classical dark cloud.

In summary, we have used the VLA and ALMA to obtain tight constraints on the O_2 abundance (relative to H_2), $X(\mathrm{O_2}) \leqslant 9.1 \times 10^{-6}$, in the $z = 0.88582$ spiral gravitational lens toward PKS 1830−21. This is a factor of $\gtrsim$15 more stringent than the best previous constraint on the O_2 abundance in an external galaxy. We argue that the low O_2 abundance in the $z \sim 0.886$ lens may arise due to its high neutral carbon abundance (resulting in the efficient destruction of O_2), and the fact that the absorbing clouds are probably not dark clouds, but instead diffuse or translucent clouds, with relatively low number density and high gas kinetic temperature.

This paper makes use of the following ALMA data: ADS/JAO.ALMA#2012.1.00581.S. ALMA is a partnership of ESO (representing its member states), NSF (USA) and NINS (Japan), together with NRC (Canada), NSC and ASIAA (Taiwan), and KASI (Republic of Korea), in cooperation with the Republic of Chile. The Joint ALMA Observatory is operated by ESO, AUI/NRAO and NAOJ. This paper also makes use of VLA data (proposal 10A-110). The National Radio Astronomy Observatory is operated by Associated Universities, Inc, under cooperative agreement with the NSF. N.K. acknowledges support from the Department of Science and Technology via a Swarnajayanti Fellowship. D.S.M. acknowledges partial support by the National Science Foundation through grant AST-1009620.

REFERENCES

Bagdonaite, J., Jansen, P., Henkel, C., et al. 2013, Sci, 339, 46
Bergin, E. A., Melnick, G. J., Stauffer, F. R., et al. 2000, ApJL, 539, L129
Bottinelli, S., Hughes, A. M., van Dishoeck, E. F., et al. 2009, ApJL, 690, L130
Charnley, S. B., Rodgers, S. D., & Ehrenfreund, P. 2001, A&A, 378, 1024
Chen, J.-H., Goldsmith, P. F., Viti, S., et al. 2014, ApJ, 793, 111
Chengalur, J. N., de Bruyn, A. G., & Narasimha, D. 1999, A&A, 343, L79
Combes, F., & Wiklind, T. 1995, A&A, 303, L61
Combes, F., & Wiklind, T. 1997, ApJL, 486, L79
Combes, F., Wiklind, T., & Nakai, N. 1997, A&A, 327, L17
Dai, X., Kochanek, C. S., Chartas, G., & Mathur, S. 2006, ApJ, 637, 53
Drouin, B. J., Yu, S., Miller, C. E., et al. 2010, JQSRT, 111, 1167
Gerin, M., Phillips, T. G., Benford, D. J., et al. 1997, ApJL, 488, L31
Goldsmith, P. F., & Langer, W. D. 1978, ApJ, 222, 881
Goldsmith, P. F., Liseau, R., Bell, T. A., et al. 2011, ApJ, 737, 96
Goldsmith, P. F., Melnick, G. J., Bergin, E. A., et al. 2000, ApJL, 539, L123
Henkel, C., Braatz, J. A., Menten, K. M., & Ott, J. 2008, A&A, 485, 451
Henkel, C., Jethava, N., Kraus, A., et al. 2005, A&A, 440, 893
Henkel, C., Menten, K. M., Murphy, M. T., et al. 2009, A&A, 500, 725
Herbst, E., & Klemperer, W. 1973, ApJ, 185, 505
Hollenbach, D., Kaufman, M. J., Bergin, E. A., & Melnick, G. J. 2009, ApJ, 690, 1497
Jin, C., Garrett, M. A., Nair, S., et al. 2003, MNRAS, 340, 1309
Kanekar, N. 2011, ApJL, 728, L12
Kanekar, N., & Chengalur, J. N. 2002, A&A, 381, L73
Kanekar, N., Chengalur, J. N., de Bruyn, A. G., & Narasimha, D. 2003, MNRAS, 345, L7
Kanekar, N., Ubachs, W., Menten, K. M., et al. 2015, MNRAS, 448, L104
Larsson, B., Liseau, R., Pagani, L., et al. 2007, A&A, 466, 999
Lidman, C., Courbin, F., Meylan, G., et al. 1999, ApJL, 514, L57
Lique, F. 2010, JChPh, 132, 044311
Liseau, R., Goldsmith, P. F., Larsson, B., et al. 2012, A&A, 541, A73
Liseau, R., Larsson, B., Bergman, P., et al. 2010, A&A, 510, A98
Lovell, J. E. J., Reynolds, J. E., Jauncey, D. L., et al. 1996, ApJL, 472, L5
Marechal, P., Pagani, L., Langer, W. D., & Castets, A. 1997, A&A, 318, 252
Mathur, S., & Nair, S. 1997, ApJ, 484, 140
Melnick, G. J., & Kaufman, M. J. 2015, ApJ, 806, 227
Menten, K. M., Güsten, R., Leurini, S., et al. 2008, A&A, 492, 725
Muller, S., Beelen, A., Black, J. H., et al. 2013, A&A, 551, 109
Muller, S., Beelen, A., Guélin, M., et al. 2011, A&A, 535, 103
Muller, S., Combes, F., Guélin, M., et al. 2014, A&A, 566, A112
Muller, S., & Guélin, M. 2008, A&A, 491, 739
Pagani, L., Olofsson, A. O. H., Bergman, P., et al. 2003, A&A, 402, L77
Pickett, H. M., Poynter, R. L., Cohen, E. A., et al. 1998, JQSRT, 60, 883
Quan, D., Herbst, E., Millar, T. J., et al. 2008, ApJ, 681, 1318
Remijan, A. J., Markwick-Kemper, A., & the ALMA Working Group on Spectral Line Frequencies 2007, BAAS, 39, #132.11
Sato, M., Reid, M. J., Menten, K. M., & Carilli, C. L. 2013, ApJ, 764, 132
Schöier, F. L., van der Tak, F. F. S., van Dishoeck, E. F., & Black, J. H. 2005, A&A, 432, 369
Whittet, D. C. B. 2010, ApJ, 710, 1009
Wiklind, T., & Combes, F. 1995, A&A, 299, 382
Wiklind, T., & Combes, F. 1996, A&A, 315, 86
Wiklind, T., & Combes, F. 1998, ApJ, 500, 129
Yıldız, U. A., Acharyya, K., Goldsmith, P. F., et al. 2013, A&A, 558, 58